A Placement Strategy for Idle Mobile Charging Stations in IoEV: From the View of Charging Demand Force

Linfeng Liu, *Member, IEEE*, Su Liu, Jiagao Wu, *Member, IEEE*, and Jia Xu, *Senior Member, IEEE*

***Abstract*— At present, mobile charging stations (MCSs) are taken as an important complement of fixed charging stations. Currently, the strategy of MCSs is to move towards the electric vehicles to be charged (EVCs) only after being requested. To shorten the charging delay of EVCs and enhance the proportion of charged EVCs, idle MCSs should actively move to the areas with large potential charging demand rather than remaining stationary. The distribution of idle MCSs in different areas should be taken into account to prevent excessive idle MCSs from moving into the same areas simultaneously. To this end, we introduce the concept of charging demand force to depict the potential charging demand of EVCs, and then propose the Placement Strategy for Idle Mobile Charging Stations (PS-IMCS). In PS-IMCS, each idle MCS can measure the potential charging demand in neighboring areas through obtaining the resultant force composed of attraction force and repulsion force, and an MDP model is specially designed to make placement decisions for idle MCSs. Extensive simulations and comparisons demonstrate the performance superiority of PS-IMCS, i.e., the charging delay of EVCs can be significantly shortened, and the proportion of charged EVCs can be effectively enhanced.**

***Index Terms*— Internet of Electric Vehicles, mobile charging station, charging demand force, placements of idle MCSs.**

I. Introduction

DUE to the increasing shortage of fuel and the pressing need to relieve the atmospheric pollution, electric vehicles (EVs) which are typically powered by batteries have been popularized rapidly [1], [2]. EVs can realize the vehicle-to-everything (V2X) communications with their wireless communication modules, and thus constituting an Internet of Electric Vehicles (IoEV) [3] (Fig. 1).

The limited battery capacity of EVs is a bottleneck which restricts the further popularity of EVs seriously, therefore providing convenient charging services is vital to EVs. At present, the main charging solutions include fixed charging stations (FCSs) and mobile charging stations (MCSs) [4], [5]. Compared with FCSs, MCSs can provide more agile charging services with lower cost, since MCSs do not require the deployment locations and can move freely. Currently, MCSs (e.g., NIO Power, Porsche Turbo, and MOBI Charger) have been gradually deployed in many cities as an important charging solution [6].

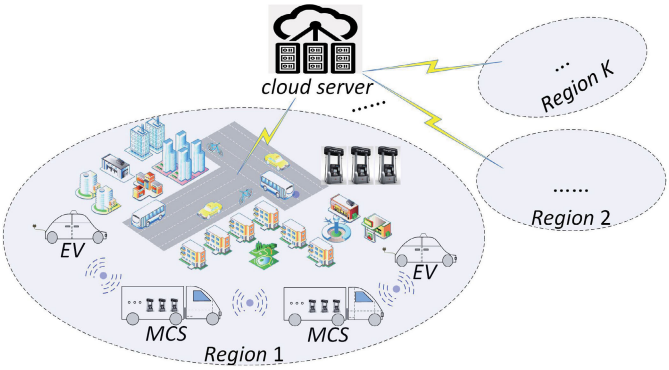

Fig. 1. An IoEV with mobile charging stations.

Typically, when the state of charge (SOC) [7] of an EV is lower than a threshold, the EV makes a charging request to the neighboring idle MCSs. After receiving the charging request, an idle MCS could move to charge the EV at a negotiated charging position. To simplify the following description, an EV to be charged by MCSs is referred to as an EVC.

MCSs are sparsely distributed in the road network (the number of MCSs is much smaller than that of EVs), implying that EVCs could be far away from idle MCSs when they make charging requests, and the charging delay of EVCs could be very large. Therefore, EVCs cannot be agilely charged by idle MCSs, if idle MCSs move towards EVCs only after being requested, i.e., idle MCSs should actively move to some new positions for the future charging. This problem motivates us to investigate the proper placements of idle MCSs, thus helping MCSs to charge EVCs timely and increase the proportion of charged EVCs.

For example, in Fig. 2 with an EVC and an idle MCS, the EVC makes a charging request to the neighboring idle MCSs when it detects a low SOC, and the EVC can be rapidly charged if an idle MCS has moved close to the EVC in advance.

Naturally, idle MCSs should actively move to the areas with large charging demand (more EVCs and/or EVCs requiring more electricity) rather than remaining stationary.

Manuscript received 7 November 2022; revised 14 April 2023, 1 August 2023, and 5 October 2023; accepted 30 October 2023. This work was supported in part by the National Natural Science Foundation of China under Grant 62272237, Grant 62372249, and Grant 61872191; and in part by the Six Talents Peak Project of Jiangsu Province under Grant 2019-XYDXX-247. The Associate Editor for this article was Y. Kim. *(Corresponding author: Jia Xu.)*

The authors are with the Jiangsu Key Laboratory of Big Data Security and Intelligent Processing, Nanjing University of Posts and Telecommunications, Nanjing 210023, China (e-mail: xujia@njupt.edu.cn).

Digital Object Identifier 10.1109/TITS.2023.3329453

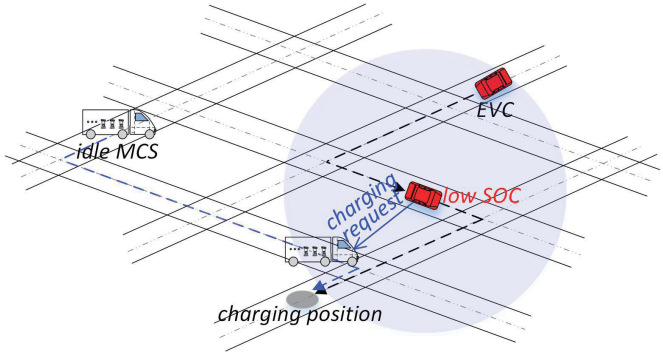

Fig. 2. An MCS charges an EVC.

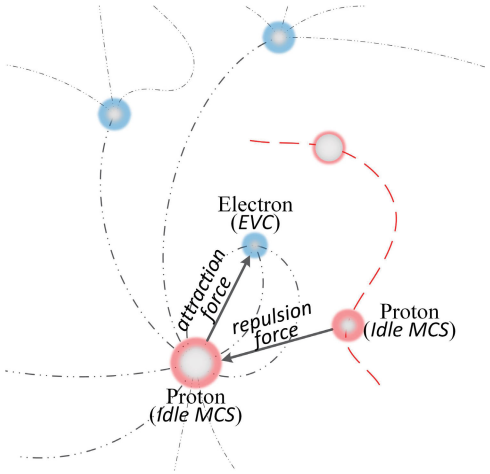

Fig. 3. The attraction force and repulsion force in nature.

The distribution of idle MCSs in different areas should be taken into account to prevent excessive idle MCSs from moving into the same areas simultaneously. Motivated by the above considerations, the concept of charging demand force is introduced to depict the potential charging demand of EVCs. Specifically, the effects of neighboring EVCs and idle MCSs on the potential charging demand around an idle MCS are mapped into the attraction force and repulsion force, respectively.

The attraction force and repulsion force are very common in nature. The attraction force denotes the force drawing or holding the particles together, and the repulsion force denotes the force causing particles to repel one another. As shown in Fig. 3, the charging demand relation between an idle MCS and a neighboring EVC is assimilated to the attraction force between a proton and an electron in nature, and the charging demand relation between two neighboring idle MCSs is assimilated to the repulsion force between two protons.

Moreover, a centralized method for the placement decisions of idle MCSs is typically not feasible, because a centralized method leads to extremely large communication overhead and computational complexity. Thus, a distributed method for the placement decisions of idle MCSs is more preferable.

In this paper, we propose a Placement Strategy for Idle Mobile Charging Stations (PS-IMCS), where each idle MCS can measure the potential charging demand in neighboring areas through obtaining the resultant force composed of attraction force and repulsion force, and a Markov decision process (MDP) model [8] is designed to make placement decisions for idle MCSs.

The remainder of this paper is organized as follows: Section II briefly surveys some existing related studies. Section III provides a system model and problem formulation for the problem of placements of idle MCSs. An MDP model for solving this problem is proposed in Section IV, and the Placement Strategy for Idle Mobile Charging Stations (PS-IMCS) is presented in Section V. Section VI covers some analyses on PS-IMCS, including the complexity, convergence, and convergence rate. Extensive simulation results for performance evaluation of PS-IMCS are reported in Section VII. Finally, Section VIII concludes this paper.

II. Related Work

A. Charging With Fixed Charging Stations

FCSs can provide the electricity replenishment for EVs at fixed charging sites with some installed charging facilities. EVs need to travel to FCSs for charging their batteries. The key considerations for FCSs are twofold: optimal layout of FCSs, and charging task arrangement.

The deployment of FCSs is quite costly, and thus the site selections for the installations of FCSs are very important. To minimize the deployment cost of FCSs and the charging delay of EVs, some research has been conducted, such as [9] and [10]. In [9], a bi-level optimization model is employed to find a virtually-optimal charging station deployment, and thus the installation cost and power losses are reduced. In [10], the optimal sites of FCSs are identified according to the estimation of the actual charging demand throughout the urban area. The proposed method can reduce the waiting time, travel time, and charging time of EVs. There are also some studies focusing on the optimal number of FCSs which should be deployed, such as [11] and [12].

As for the charging task arrangement, the major concern is that how to schedule EVs to improve the charging efficiency of FCSs. Due to the different charging demand during different time intervals, some existing literatures investigate the pricing strategies based on the interactions between EVs and FCSs, and the typical works include [13], [14], where the charging price is adaptively adjusted during peak hours and off-peak hours. Reference [13] defines the price elasticity by a linear demand-price function. The aggregated charging of unoccupied EVs is scheduled in each parking lot to maximize the charging profit, and the electricity consumption is paid at the locational marginal price. To achieve the effective use of FCSs, the dynamic pricing problem is formulated into a mixed competitive-cooperative multi-agent reinforcement learning task in [14]. A shared meta generator is provided to generate individual customized dynamic pricing policies for diverse agents, and hence the utilization of all FCSs is improved.

B. Charging With Mobile Charging Stations

Due to the capability of mobility, MCSs can offer charging services more agilely, and the number of deployed MCSs has been increasing in recent years [15].

MCSs can deliver the electricity from FCSs or power grid to EVCs conveniently, and some research has been conducted. For example, in [6] an intelligent mobile charging control mechanism termed R-COST is provided for EVCs, by promoting the charging reservations (service start time, expected charging time, and charging location). Reference [16] presents an optimization framework where an MCS can be dispatched to an overloaded FCS to reduce the number of waiting EVs. Some models or methods have been adopted to solve the scheduling problem of MCSs, such as Stackelberg game [17], and mixed integer optimization model [18]. A parallel mobile charging service is proposed in [18] to schedule MCSs to charge EVs at their parking spots, and each MCS is allowed to charge multiple EVs simultaneously. Due to the heavy traffic and the constraints of charging locations, an operational mode through temporarily stationing MCSs at different places is proposed in [19]. A dynamic charging scheduling scheme for MCSs is given by [20] to realize the fast responses, reduce the electricity consumption, and improve the charging efficiency. Likewise, an assignment rescheduling mechanism of MCSs is presented to reduce the charging expenses of EVs and enhance the proportion of charged EVs [21]. In [22], the scheduling of MCSs is modeled as an MDP problem which is solved by a reinforcement learning method. Reference [23] investigates the fleet management of electricity providers, and the minimum number of electricity providers dispatched to serve the electric vehicles is analyzed.

As a similar problem, the problem of relocating idle vehicles has been studied. For example, [24] proposes a queueing-based formulation to depict this problem in an on-demand mobility service, and the proposed algorithm can reduce the relocation cost largely. Specially, the projection from a continuously updated vector field of taxi travel momentum to the points of interest can be generated by [25]. For the vehicle-sharing operations, a rebalancing policy using cost function approximation is presented in [26], and the cost function is modeled as a p-median relocation problem with the minimum cost flow conservation.

Typically, the destinations and future routes of EVs cannot be provided to MCSs due to the privacy protection of EV drivers. Thus, the unpredictability in the future movements of EVCs makes MCSs difficult to quickly respond to the charging requests of EVCs, which could lead to the long waiting time and large charging expenses of EVCs. This issue has not been considered in the above works.

C. Attraction Force and Repulsion Force

The attraction-repulsion model has been applied in some research [27], [28], [29], [30]. In [27], Kang et al. investigate an attraction-repulsion Keller-Segel system with a degradation source of a sub-quadratic power in a bounded domain. In [28], a weighted superposition attraction-repulsion mechanism based on meta-heuristic algorithm is proposed to achieve a superior balance between solution accuracy and computational cost. Depending on the tendencies of attraction force and repulsion force between members, [29] presents a performance improvement for a flocking task with an unknown target zone. Moreover, [30] gives a graph contrastive learning network for unsupervised domain adaptive graph learning, which is based on the concepts of attraction force and repulsion force. An attraction force encourages the node features from two domains to be largely consistent, whereas a repulsion force ensures that the node features are discriminative to differentiate the graph domains.

The attraction-repulsion model can depict the interaction between charging demand and charging supply in areas over time, and thus can measure the potential charging demand of EVCs in future. At present, to the best of our knowledge, the attraction-repulsion model has not been applied to measure the potential charging demand of EVCs and help to make placement decisions for idle MCSs.

D. Motivation of Our Work

Without the private information of EVCs (e.g., destinations, future routes), idle MCSs usually track the EVCs with larger charging demand and move into the areas with few idle MCSs (smaller charging supply). To offer agile charging services, the proper placement decisions should be made for idle MCSs. We measure the potential charging demand according to the resultant force which is composed of the following two parts: the attraction force reflecting the potential charging demand of EVCs, and the repulsion force reflecting the potential charging supply of idle MCSs.

Note that a centralized strategy is not feasible for the placement decisions of idle MCSs due to the extremely large communication complexity and computational complexity, and a distributed strategy is more preferable. Thus, in this work each idle MCS independently measures the potential charging demand in the neighboring area. MDP is a discrete-time stochastic control process which can model the decision making in situations where outcomes are partly random and partly under the control of decision makers. Therefore, an MDP model is applied for the problem formulation and the local placement decisions of idle MCSs.

III. System Model and Problem Formulation

The road network in the 2D plane is denoted by $\mathcal{L}$ (as shown in Fig. 4). In $\mathcal{L}$, there are N EVs and M MCSs. The set of EVs and the set of MCSs are denoted by $\mathcal{E} = \{v_1, \cdots, v_N\}$ and $\mathcal{M} = \{\varphi_1, \cdots, \varphi_M\}$, respectively. The location set of charging parks is denoted by $\boldsymbol{P}$, and the charging positions and the placements of idle MCSs are selected from $\boldsymbol{P}$. Time is divided into discrete time slots with an equal length of t_s. The current position and residual electricity are detected by each EV every time slot, and the placement decision of each idle MCS is made every time slot as well.

Several definitions are first given to depict the problem of placements of idle MCSs:

Definition 1 (Electric Vehicles): Each EV (each MCS) has the same communication range R_c. For an EV v_i, v_i travels at a speed of $m_s(v_i)$ from the departure position o_i to the destination d_i, and c unit of battery electricity is consumed for travelling through a unit distance.

In the t-th time slot, the current position and the residual battery electricity are denoted by $p(v_i)^{(t)}$ and $e(v_i)^{(t)}$,

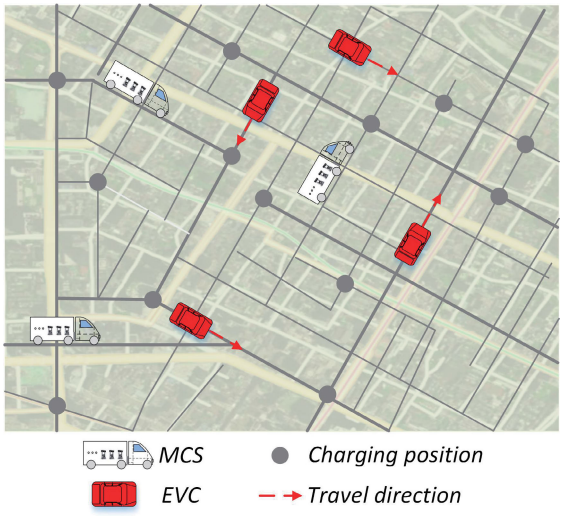

Fig. 4. A road network with EVCs and MCSs.

respectively. When v_i detects a low battery state (e.g., $e(v_i)^{(t)} \leq \frac{e(v_i)^{(0)}}{\gamma}$), v_i turns into an EVC.

Definition 2 (Mobile Charging Stations): The travel speed of an MCS φ_j is denoted by $m_s(\varphi_j)$. In the t-th time slot, the current position and the residual electricity[1] (which can be provided to EVCs) of φ_j are denoted by $p(\varphi_j)^{(t)}$ and $e(\varphi_j)^{(t)}$, respectively. e_{max} denotes the maximum battery capacity of each MCS, i.e., the residual electricity of an MCS is equal to e_{max} after it is recharged by the power grid. The charging speed of each MCS is marked by ϖ, and c unit of battery electricity is consumed for travelling through a unit distance.

An MCS that receives and approves a charging request (from an EVC) is a busy MCS, and an MCS that does not receive or approve a charging request is an idle MCS. Each MCS can obtain the information of its current position and residual electricity. Moreover, every time slot each idle MCS can also obtain the current positions and the required electricity of neighboring EVCs, the current positions and the residual electricity of neighboring idle MCSs. However, the destinations and future routes of EVCs, the historical trajectories of EVCs and other MCSs, are not provided to the idle MCS due to the privacy protection.

Definition3 (An MCS charges an EVC):. Suppose an MCS φ_j is assigned to charge an EVC v_i at the position $\widehat{p}$, and then the extra travel distance of v_i is calculated by:

$$L(v_i, \widehat{p}) = \mathscr{D}(p(v_i)^{(t)}, \widehat{p}) + \mathscr{D}(\widehat{p}, d_i) - \mathscr{D}(p(v_i)^{(t)}, d_i), \quad (1)$$

where $\mathscr{D}(p(v_i)^{(t)}, \widehat{p})$ denotes the travel distance from $p(v_i)^{(t)}$ to $\widehat{p}$. The amount of electricity required by v_i (i.e., the amount of electricity transferred from φ_j to v_i) is expressed as:

$$E(v_i, \widehat{p}) = c \cdot \{\mathscr{D}(o_i, d_i) + L(v_i, \widehat{p})\} - e(v_i)^{(0)}. \quad (2)$$

Then, the residual electricity of MCS φ_j is reduced by $E(v_i, \widehat{p}) + c \cdot \mathscr{D}(p(\varphi_j)^{(t)}, \widehat{p})$ after it has charged EVC v_i.

[1]The battery capacity of MCSs is limited as well, and MCSs will be unavailable due to the lack of electricity. The MCSs lacking electricity should be recharged by FCSs or power grid.

The charging delay of v_i is computed by:

$$Delay(v_i) = \frac{L(v_i, \widetilde{p})}{m_s(v_i)} + T_w(v_i, \varphi_j, \widehat{p}) + \frac{E(v_i, \widehat{p})}{\varpi}, \quad (3)$$

which indicates that the charging delay of v_i is comprised of: (i) The delay for the extra travel of v_i; (ii) The delay for waiting the arrival of φ_j (when v_i arrives at the charging position prior to φ_j); (iii) The delay for transferring electricity from φ_j to v_i. Specifically, $T_w(v_i, \psi_j, \widehat{p})$ is computed as [21]:

$$T_w(v_i, \varphi_j, \widehat{p}) = \begin{cases} 0, \\ \quad \text{if } \frac{\mathscr{D}(p(v_i)^{(t)}, \widehat{p})}{m_s(v_i)} \geq \frac{\mathscr{D}(p(\varphi_j)^{(t)}, \widehat{p})}{m_s(\varphi_j)}, \\ \frac{\mathscr{D}(p(\varphi_j)^{(t)}, \widehat{p})}{m_s(\varphi_j)} - \frac{\mathscr{D}(p(v_i)^{(t)}, \widehat{p})}{m_s(v_i)}, \\ \quad \text{otherwise.} \end{cases} \quad (4)$$

If the waiting delay $T_w(v_i, \varphi_j, \widehat{p})$ is larger than the maximum waiting delay $\widetilde{D}$, and then it is regarded as a charging failure, i.e., the assigned MCS φ_j fails to charge the EVC v_i. Likewise, the waiting delay of the assigned MCS φ_j is calculated as

$$T_w(\varphi_j, v_i, \widehat{p}) = \begin{cases} 0, \\ \quad \text{if } \frac{\mathscr{D}(p(v_i)^{(t)}, \widehat{p})}{m_s(v_i)} < \frac{\mathscr{D}(p(\varphi_j)^{(t)}, \widehat{p})}{m_s(\varphi_j)}, \\ \frac{\mathscr{D}(p(v_i)^{(t)}, \widehat{p})}{m_s(v_i)} - \frac{\mathscr{D}(p(\varphi_j)^{(t)}, \widehat{p})}{m_s(\varphi_j)}, \\ \quad \text{otherwise,} \end{cases}$$

and if $T_w(\varphi_j, v_i, \widehat{p})$ is larger than $\widetilde{D}$, then there is a charging failure as well.

Definition 4 (Charging Demand Force):. Each idle MCS measures the potential charging demand in the neighboring area through obtaining the resultant force composed of attraction force and repulsion force. For an idle MCS φ_j, the sets of neighboring EVCs and neighboring idle MCSs are denoted by $\mathcal{E}_n(\varphi_j)$ and $\mathcal{M}_n(\varphi_j)$, respectively. $\mathcal{E}_n(\varphi_j) = \{v_i \in \mathcal{E} |\ dis(\varphi_j, v_i) \leq R_c\}$ and $\mathcal{M}_n(\varphi_j) = \{\varphi_{j'} \in \mathcal{M} |\ dis(\varphi_j, \varphi_{j'}) \leq R_c\}$, where $dis(\varphi_j, v_i)$ denotes the Euclidean distance between φ_j, and v_i.

In essence, an idle MCS should move to the areas with larger charging demand, i.e., in the areas there are more EVCs requiring more electricity (larger charging requirement) and fewer idle MCSs with less residual electricity (smaller charging supply). As shown in Fig. 3, an idle MCS is assimilated to a positive proton, and the mass of the idle MCS is measured by its residual electricity. Likewise, an EVC is assimilated to a negative electron, and the mass of the EVC is measured by its required electricity. Thus, an idle MCS is repulsed by neighboring idle MCSs and attracted by neighboring EVCs.

A neighboring EVC v_i ($v_i \in \mathcal{E}_n(\varphi_j)$) produces the attraction force to φ_j:

$$\overrightarrow{F}_a(\varphi_j, v_i)^{(t)} = \frac{\{c \cdot \mathscr{D}(o_i, d_i) - e(v_i)^{(0)}\} \cdot e(\varphi_j)^{(t)}}{\mathscr{D}(p(\varphi_j)^{(t)}, p(v_i)^{(t)})^3} \cdot \overrightarrow{\varphi_j v_i}, \quad (5)$$

where $\overrightarrow{\varphi_j v_i}$ denotes a direction vector. Likewise, a neighboring idle MCS $\varphi_j{}'$ ($\varphi_j{}' \in \mathcal{M}_n(\varphi_j)$) produces the repulsion force to φ_j:

$$\overrightarrow{F}_r(\varphi_j{}', \varphi_j)^{(t)} = \frac{e(\varphi_j{}')^{(t)} \cdot e(\varphi_j)^{(t)}}{\mathscr{D}(p(\varphi_j{}')^{(t)}, p(\varphi_j)^{(t)})^3} \cdot \overrightarrow{\varphi_j{}'\varphi_j}, \quad (6)$$

which indicates that the repulsion effect becomes larger when the idle MCSs (with more residual electricity) become closer. By this mechanism, the idle MCSs with more residual electricity will not be located very close, and the charging capacity of idle MCSs can be balanced among areas.

Then, the resultant force of φ_j is obtained by:

$$\overrightarrow{F}(\varphi_j)^{(t)} = \sum_{v_i \in \mathcal{E}_n(\varphi_j)} \overrightarrow{F}_a(\varphi_j, v_i)^{(t)} + \sum_{\varphi_j{}' \in \mathcal{M}_n(\varphi_j)} \overrightarrow{F}_r(\varphi_j{}', \varphi_j)^{(t)}. \quad (7)$$

Note that the charging demand force is obtained without the information of the destinations and future routes of EVCs, and thus the privacy of EVCs can be protected.

To shorten the charging delay of EVCs and enhance the proportion of charged EVCs, the problem objective of placements of idle MCSs is formally provided as follows:

$$\begin{cases} \min \ \dfrac{\sum_{i=1}^{N_e} Delay(v_i)}{N_e}, \\ \max \ \dfrac{N_c}{N_e}, \end{cases} \quad (8)$$

where N_e and N_c denote the number of EVCs and the number of charged EVCs, respectively. The objective of the minimization of the charging delay of EVCs enables MCSs to charge EVCs as quickly as possible, implying that more EVCs can be quickly charged (the proportion of charged EVCs is increased). In essence, these two objectives can shorten the extra travels of EVCs and promote the charging efficiency of MCSs.

In the next section, we will propose a Placement Strategy for Idle Mobile Charging Stations (PS-IMCS) to make placement decisions for idle MCSs. In PS-IMCS, the concept of charging demand force is introduced, and each idle MCS can measure the potential charging demand in the neighboring area through obtaining the resultant force (charging demand force) which is composed of attraction force and repulsion force. Specially, based on the potential charging demand, an MDP model is designed to make placement decisions for idle MCSs. By PS-IMCS, more EVCs can be promptly charged by MCSs.

IV. Markov Decision Process for Placements of Idle MCSs

The statuses of EVs and MCSs are varied over time: An EV turns into an EVC when it detects a low battery state, and an EVC reverts back to an EV when it has been charged. An idle MCS can be assigned to charge an EVC, and an MCS in the charging status turns into an idle MCS after charging the EVC.

As aforementioned above, the destinations and future routes of EVCs are not provided to MCSs due to the privacy protection, and thus idle MCSs are difficult to track and charge EVCs according to the future travel routes of EVCs, which indicates that the potential charging demand around each idle MCS is unpredictable. The potential charging demand in the current time slot should be evaluated by exploiting that in the last time slot (rather than during the more previous time slots). Therefore, an MDP is introduced to formulate the problem of placements of idle MCSs, and help to make placement decisions for them.

A. Markov Decision Process

An MDP model for formulating the problem of placements of idle MCSs is represented by a quintuple $< \mathcal{S}, \mathcal{A}, \mathcal{T}, \mathcal{P}, \mathcal{R} >$. For an idle MCS φ_j, the quintuple is explained as follows:

(i) $\mathcal{S}$ denotes the set of states of idle MCSs, where a state indicates the potential charging demand around an idle MCS, which also implies that how far away is the optimal placement from the current position of the idle MCS. For example, in the t-th time slot, the state of an idle MCS φ_j is written as:

$$s_t = \left[\left| \overrightarrow{F}(\varphi_j)^{(t)} \right| \right], \quad (9)$$

where $|\cdot|$ denotes the vector value, and $[\cdot]$ denotes an integral operation. Thus, the value of states is discrete, and the number of states is finite because the maximum resultant force is limited.

(ii) $\mathcal{A}$ denotes the set of actions of idle MCSs, where an action denotes a possible placement of an idle MCS. Each placement is selected from the location set of charging parks. The set of actions of an idle MCS is expressed by (17) in Section IV-B.

(iii) $\mathcal{T} = \{1, \cdots, t, \cdots, T\}$ is a finite set of time slots, because the maximum battery capacity of MCSs is limited.

(iv) $\mathcal{P} = \{\mathscr{P}(s_{t+1}|s_t, a_t)\}_{1 \le t \le T-1}$ denotes a transition probability matrix, and the element $\mathscr{P}(s_{t+1}|s_t, a_t)$ is expressed as:

$$\mathscr{P}(s_{t+1}|s_t, a_t) = \frac{\left| \overrightarrow{F}(\varphi_j)^{(t+1)} \right|}{\sum_{a \in A(\varphi_j)^{(t)}} \left| \overrightarrow{F}(\varphi_j(a))^{(t+1)} \right|}, \quad (10)$$

where $\overrightarrow{F}(\varphi_j(a))^{(t+1)}$ denotes the resultant force of φ_j in the $(t+1)$-th time slot (after φ_j adopts the action a_t in the t-th time slot). (10) transits the potential charging demand into the placement probability of idle MCSs, i.e., (10) measures the probability of the variation of potential charging demand by adopting an action a_t.

(v) $\mathcal{R} = \{r_1, \cdots, r_t, \cdots, r_T\}$ denotes the set of immediate rewards, where the immediate reward of φ_j in the $(t+1)$-th time slot is calculated by:

$$r_{t+1} = \left| \overrightarrow{F}(\varphi_j)^{(t+1)} \right| - \left| \overrightarrow{F}(\varphi_j)^{(t)} \right|. \quad (11)$$

The cumulative reward after the t-th time slot is given by:

$$G_t = \sum_{k=0}^{T-1} \varsigma^k \cdot r_{t+k+1}, \quad (12)$$

where ς is a discount coefficient.

A value function $V(s_t, a_t)$ is defined to denote the expected value of G_t, i.e., $V(s_t, a_t) = \mathbb{E}[G_t | s_t = s, a_t = a]$. Then, a Bellman equation can be extrapolated:

$$V(s_t, a_t) = r_{s_t}^{a_t} + \varsigma \cdot \sum_{s_{t+1}} \{\mathscr{P}(s_{t+1}|s_t, a_t) \cdot V(s_{t+1}, a_{t+1})\}. \tag{13}$$

In (13), $r_{s_t}^{a_t}$ denotes the immediate reward by adopting the action a_t under the state s_t (in the t-th time slot). $r_{s_t}^{a_t}$ also represents the expected value of r_{t+1}, and is expressed as $r_{s_t}^{a_t} = \mathbb{E}(r_{t+1}|s_t, a_t)$.

Therefore, the optimal action a_t^* can be obtained by:

$$a_t^* = \arg \max_{a \in A(\varphi_j)^{(t)}} V(s_t, a). \tag{14}$$

There must be an optimal solution in (14), which is proved by Lemma 1.

Lemma 1: There exists an optimal solution in our proposed MDP model.

Proof: ($\mathbb{X}$,L-infinity) denotes a metric space, and $\mathbb{X}$ denotes the set of real numbers ($\mathbb{X} \in \mathbb{R}$). The output of value functions belongs to $\mathbb{X}$. L-infinity is defined by:

$$\|\mathbb{X}\|_\infty = \max_{i \in [0, |\mathbb{X}|]} |\mathbb{X}_i|.$$

The Bellman operator B is defined by:

$$BV(s_t, a_t) = \max_{a_t \in A(\varphi_j)^{(t)}} \left\{ r_{s_t}^{a_t} + \varsigma \cdot \sum_{s_{t+1}} \left[\mathscr{P}(s_{t+1}|s_t, a_t) \cdot v(s_{t+1}, a_{t+1}) \right] \right\}.$$

By the Banach fixed point theorem [31], if we can obtain the following two conditions: (i) ($\mathbb{X}$,L-infinity) is a complete metric space, and (ii) the Bellman operator B is a contractor in the finite space ($\mathbb{R}$,L-infinity). Then, we can conclude that there exists an optimal solution in the MDP model.

(i) ($\mathbb{X}$,L-infinity) is a complete metric space. The distance between the two value functions is equal to the highest element-wise absolute difference between the two value functions. The rewards are finite in the MDP model, and then the value functions will always stay in the real space, therefore this finite space will always be complete.

(ii) The Bellman operator B is a contractor in the finite space ($\mathbb{R}$,L-infinity). For any two value functions V_1 and V_2, we have that:

$$\begin{aligned}
&\|BV_1(s_t, a_t) - BV_2(s_t, a_t)\| \\
&= \left\| \max_{a_t} \left\{ r_{s_t}^{a_t} + \varsigma \cdot \sum_{s_{t+1}} \left[\mathscr{P}(s_{t+1}|s_t, a_t) \cdot vV_1(s_{t+1}, a_{t+1}) \right] \right\} \right\| \\
&\quad - \left\| \max_{a_t} \left\{ r_{s_t}^{a_t} + \varsigma \cdot \sum_{s_{t+1}} \left[\mathscr{P}(s_{t+1}|s_t, a_t) \cdot V_2(s_{t+1}, a_{t+1}) \right] \right\} \right\| \\
&\le \varsigma \cdot \left\| \max_{a_t} \left\{ \sum_{s_{t+1}} \left[\mathscr{P}(s_{t+1}|s_t, a_t) \cdot \begin{pmatrix} V_1(s_{t+1}, a_{t+1}) \\ -V_2(s_{t+1}, a_{t+1}) \end{pmatrix} \right] \right\} \right\| \\
&\le \varsigma \cdot \|V_1(s_{t+1}, a_{t+1}) - V_2(s_{t+1}, a_{t+1})\| \\
&\quad \cdot \max_{a_t} \sum_{a_t, s_{t+1}} \mathscr{P}(s_{t+1}|s_t, a_t) \\
&< \varsigma \cdot \|V_1(s_{t+1}, a_{t+1}) - V_2(s_{t+1}, a_{t+1})\|,
\end{aligned}$$

where there is $0 < \varsigma < 1$, and then the Bellman operator B is a contractor in the finite space ($\mathbb{R}$, L-infinity).

Thus, by the Banach fixed point theorem, we conclude that there exists an optimal solution in the MDP model. □

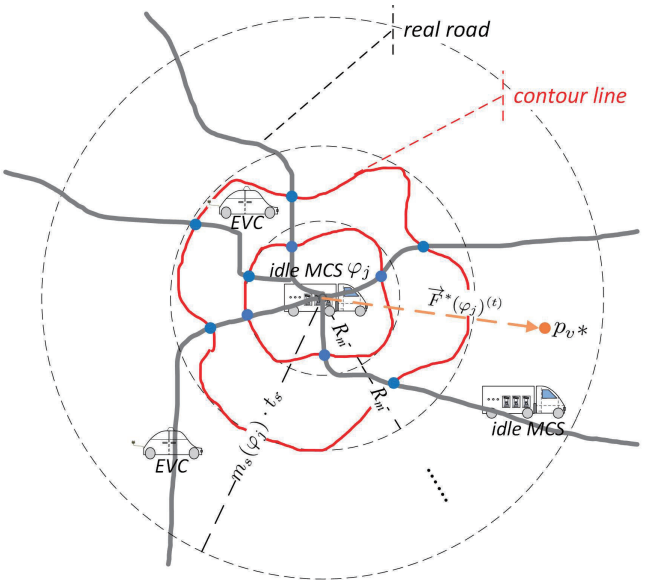

Fig. 5. Division of the circular range around an idle MCS.

B. Actions of Idle MCSs

Note that the potential actions of an idle MCS φ_j could be time-varying, and a gradient force model is introduced to calculate the set of actions $A(\varphi_j)^{(t)}$.

The maximum travel distance of φ_j during a time slot is $m_s(\varphi_j) \cdot t_s$, and the circular range with the radius $m_s(\varphi_j) \cdot t_s$ is equally divided into χ virtual layers with the radius $R_m = \frac{m_s(\varphi_j) \cdot t_s}{\chi}$, as illustrated in Fig. 5, where φ_j is taken as the center, and the circular areas with the radii $R_m, 2R_m, \cdots, m_s(\varphi_j) \cdot t_s$ are denoted by $\phi_1, \phi_2, \cdots, \phi_\chi$, respectively.

In Fig. 5, a contour line in red is generated by the positions (on the real roads) with the same travel distance $(R_m, 2R_m, \cdots, m_s(\varphi_j) \cdot t_s)$ to φ_j.

Then, the maximum resultant force of φ_j is obtained by:

$$\vec{F}^*(\varphi_j)^{(t)} = \max_{1 \le k \le \chi} \left\{ \sum_{v_i \in \phi_k} \vec{F}_a(\varphi_j, v_i)^{(t)} + \sum_{\varphi_j' \in \phi_k} \vec{F}_r(\varphi_j', \varphi_j)^{(t)} \right\}. \tag{15}$$

Furthermore, the optimal virtual placement p_v^* can be found by:

$$p_v^* = \frac{\vec{F}^*(\varphi_j)^{(t)}}{\left|\vec{F}^*(\varphi_j)^{(t)}\right|} \cdot \left\{ m_s(\varphi_j) \cdot t_s \cdot \frac{k + 0.5}{\chi} \right\}, \tag{16}$$

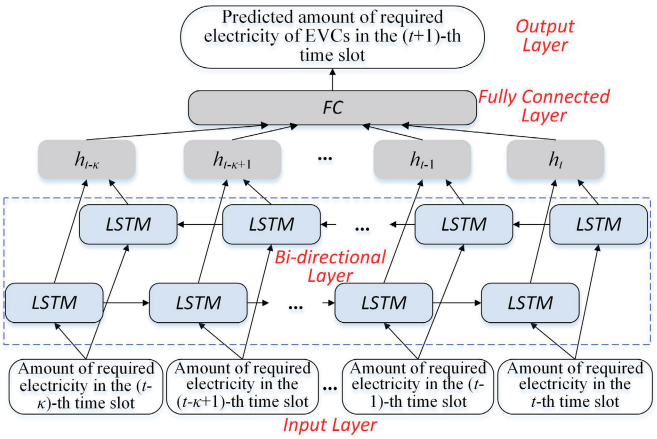

Fig. 6. Bi-LSTM model for predicting the amount of required electricity of EVCs on a road segment.

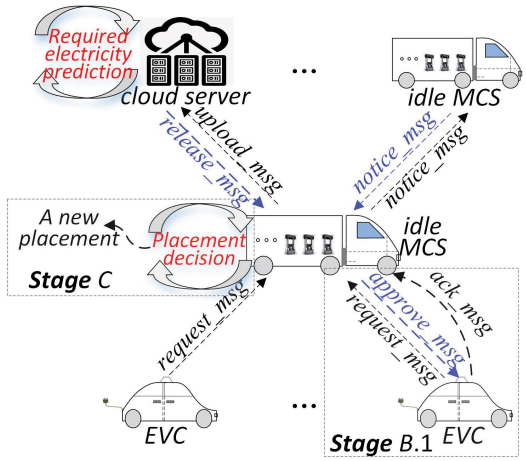

Fig. 7. Message exchanges in PS-IMCS.

which indicates that the optimal virtual placement is selected from the layer where the maximum resultant force $\overrightarrow{F}^*(\varphi_j)^{(t)}$ is obtained.

The set of actions of φ_j is expressed as:

$$A(\varphi_j)^{(t)} = \left\{a |\ a \in \boldsymbol{P}, dis(p_v^*, a) \leq 2R_m\right\}. \tag{17}$$

where $dis(p_v^*, a)$ denotes the Euclidean distance between p_v^* and a.

C. States Transitions of Idle MCSs

The resultant force of an idle MCS is related to the real-time positions of neighboring EVCs. With regard to each road segment, the amount of required electricity of EVCs on the road segment (in the previous κ time slots) is fed into a Bi-LSTM model [32], because Bi-LSTM has an excellent generalization ability, and it performs well in the prediction of time series, such as the amount of required electricity of EVCs which is continuously varied. Thus, the future amount of required electricity of EVCs on the road segment can be predicted, as shown in Fig. 6.

By the predicted amount of required electricity of EVCs on road segments, the resultant attraction force on each road segment is introduced to simplify the problem analysis, i.e., the attraction force of the EVCs on the same road segment is synthetically calculated, based on the assumption that the EVCs on the same road segment have the same distance to the idle MCS. For example, the attraction force of an idle MCS φ_j in the $(t+1)$-th time slot is written as:

$$\sum_{l \in \mathcal{L}} \left\{ \frac{E(l)^{(t+1)} \cdot e(\varphi_j)^{(t)}}{\mathscr{D}(p(\varphi_j)^{(t)}, \ddot{p}(l))^3} \cdot \overrightarrow{\varphi_j \ddot{p}(l)} \right\},$$
$$s.t.\ \mathscr{D}(p(\varphi_j)^{(t)}, \quad \ddot{p}(l)) \leq m_s(\varphi_j) \cdot t_s, \tag{18}$$

where $E(l)^{(t+1)}$ denotes the predicted amount of required electricity of EVCs on the road segment l in the $(t+1)$-th time slot, and $\ddot{p}(l)$ denotes the midpoint of the road segment l.

Then, the resultant force and the transition probability matrix can be obtained by (7) and (10), respectively.

V. Placement Strategy for Idle Mobile Charging Stations

To shorten the charging delay of EVCs and enhance the proportion of charged EVCs, idle MCSs should actively track the EVCs with large charging demand and move into the areas with small charging supply. Then, the proper placement decisions can be made for idle MCSs by our proposed MDP model. The main stages of PS-IMCS are described as follows:

Stage *A. EVCs Make Charging Requests to Idle MCSs.* In each time slot (suppose the t-th time slot), if an EVC v_i makes a charging request by broadcasting a $request\_msg$ message within the communication range R_c (Fig. 7).

The $request\_msg$ of v_i includes the current position and the required electricity, and is expressed as $(p(v_i)^{(t)}, \Delta e(v_i))$, where $\Delta e(v_i)$ is calculated by:

$$\Delta e(v_i) = c \cdot \mathscr{D}(o_i, d_i) - e(v_i)^{(0)}. \tag{19}$$

Stage *B. Idle MCSs Approve the Charging Requests of EVCs.* After an idle MCS φ_j receives the $request\_msg$ from v_i, $(p(v_i)^{(t)}, \Delta e(v_i))$ is encapsuled into an $upload\_msg$ message (Fig. 7) and then is uploaded to the cloud server for predicting the amount of required electricity of EVCs. If φ_j accepts the charging request of v_i, an $approve\_msg$ message (Fig. 7) is sent back to v_i.

Specifically, in *Stage B*, the following cases are discussed:

- *Case* 1: An EVC makes a charging request to an idle MCS. The idle MCS approves the charging request of the EVC.
- *Case* 2: Multiple EVCs make charging requests to the same idle MCS (some EVCs compete for the MCS). The idle MCS approves the charging request of the EVC with the largest required electricity by the received $request\_msg$ messages.
- *Case* 3: An EVC makes a charging request to multiple idle MCSs. These idle MCSs could send several $approve\_msg$ messages to the EVC, and the EVC sends an ack_msg message to the idle MCS with the shortest charging delay.

Note that the cloud server adopts a centralized learning for the prediction of the amount of required electricity on each

road segment, because a distributed learning method on MCSs or EVCs will result in the heavy communication overhead (the massive information collection of historical amount of required electricity, and the massive information release of predicted amount of required electricity).

Stage *B*.1. *MCSs charge EVCs*. When v_i receives the *approve_msg* from φ_j. The charging position $\widehat{p}$ is determined by minimizing the charging delay of v_i:

$$\widehat{p} = \arg\min_{\widetilde{p}\in \boldsymbol{P}} \left\{ Delay(v_i) |\ c \cdot \mathscr{D}(p(v_i)^{(t)}, \widetilde{p}) \le e(v_i)^{(t)} \right\}, \tag{20}$$

where $c \cdot \mathscr{D}(p(v_i)^{(t)}, \widetilde{p}) \le e(v_i)^{(t)}$ implies that the residual electricity of v_i can support the travel to the position $\widetilde{p}$.

Then, an *ack_msg* message including the charging position $\widehat{p}$ is sent to φ_j, as shown in Fig. 7. After that, v_i and φ_j move towards the charging position $\widehat{p}$ for the charging.

Stage *B*.2. *EVCs Continue their Travels*. After being charged, the EVC v_i turns into an EV, and continues the travel to the destination d_i.

Stage *C*. *Idle MCSs Decide on the Placements*. Every time slot, the cloud server releases the predicted amount of required electricity of EVCs on each road segment to idle MCSs, and thus the attraction force of each idle MCS can be calculated, as introduced in Section IV-C.

Each idle MCS exchanges a *notice_msg* message with neighboring idle MCSs (the *notice_msg* message includes the current position and the residual electricity), and then the repulsion force (charging demand force) of the idle MCS can be calculated.

If an idle MCS φ_j does not receive any charging requests from EVCs in the t-th time slot, φ_j decides on the optimal placement in the $(t+1)$-th time slot $p(\varphi_j)^{(t+1)}$ by (14), and then φ_j moves towards $p(\varphi_j)^{(t+1)}$.

An example of sequential diagram concerning the message exchanges in PS-IMCS is illustrated in Fig. 8, where two idle MCSs φ_j and $\varphi_{j'}$ receive the charging requests from an EVC v_i. φ_j is assigned to charge v_i, and $\varphi_{j'}$ moves towards a decided placement.

VI. Theoretical Analysis of PS-IMCS

A. Complexity

TABLE I shows the communication complexity and computational complexity of our proposed PS-IMCS.

With regard to the communication complexity: (i) In *Stage A*, each EVC broadcasts a *request_msg* message, and the number of *request_msg* messages is at most $\mathrm{O}(M \cdot N)$. (ii) In *Stage B*, the amounts of required electricity of neighboring EVCs are uploaded by idle MCSs to the cloud server, and the number of *upload_msg* messages reaches $\mathrm{O}(M)$. Likewise, *approve_msg* messages could be sent back to EVCs, and the number of *approve_msg* messages is $\mathrm{O}(M)$ in the worst case where each idle MCS accepts the charging request of an EVC. In *Stage B*.1, the charging positions determined by EVCs are sent to idle MCSs before the charging, and the number of *ack_msg* messages containing the charging positions is at most $\mathrm{O}(M)$. (iii) In *Stage C*, the information exchanges should be carried out between the neighboring idle MCSs, and the number of exchanged *notice_msg* messages is up to $\mathrm{O}(M^2)$.

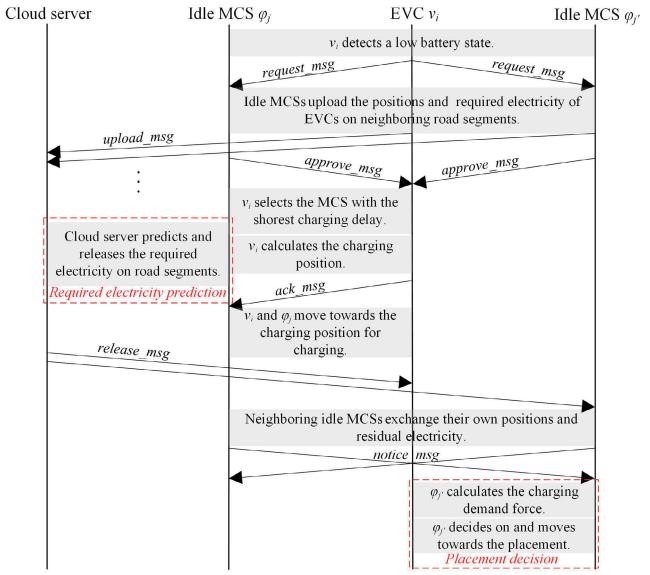

Fig. 8. Sequential diagram of PS-IMCS.

TABLE I
Complexity of PS-IMCS

Stage	Communication complexity	Computational complexity
A	$\mathrm{O}(M \cdot N)$	$\mathrm{O}(N)$
B	$\mathrm{O}(M)$	0
$B.1$	$\mathrm{O}(M)$	$\mathrm{O}(N_p \cdot N)$
$B.2$	0	0
C	$\mathrm{O}(M^2)$	$\mathrm{O}(K_c \cdot K_{in} + K_c^2 + K_c \cdot K_{out})$ +$\mathrm{O}(M)$
Total	$\mathrm{O}(M \cdot N)$	$\mathrm{O}(N_p \cdot N)$

With regard to the computational complexity: (i) Each EVC could calculate the required electricity in *Stage A*, and the computational complexity is $\mathrm{O}(N)$. (ii) Each EVC could determine the charging position (*Stage B*.1), and the computational complexity of *Stage B*.1 is at most $\mathrm{O}(N_p \cdot N)$, where N_p denotes the number of available positions which are arranged for MCSs charging EVCs. (iii) In *Stage C*, to make the placement decisions for idle MCSs, the cloud server predicts the amounts of required electricity on road segments, and the computational complexity of training the Bi-LSTM model is approximatively written as $\mathrm{O}(K_c \cdot K_{in} + K_c^2 + K_c \cdot K_{out})$, where $K_c \cdot K_{in}$ denotes the number of weights from input layer to hidden layer, K_c^2 denotes the number of weights in hidden layer, and $K_c \cdot K_{out}$ denotes the number of weights from hidden layer to output layer [33]. Each idle MCS calculates the attraction force and repulsion force, which results in $\mathrm{O}(M)$ computations.

Typically $M \ll N$, the communication complexity of PS-IMCS is of $\mathrm{O}(M \cdot N)$, and the computational complexity of PS-IMCS is of $\mathrm{O}(N_p \cdot N)$.

B. Convergence and Convergence Rate of MDP Model in PS-IMCS

Proposition 1 and Proposition 2 prove the convergence and the convergence rate of our proposed MDP model, respectively.

Proposition 1: The MDP model can converge in the Cesàro sense.

Proof: Suppose $\mathcal{P}$ is a stochastic matrix, and $\|\mathcal{P}\|$ is defined as $\|\mathcal{P}\| = \sup_i \sum_j p_{ij}$.

For an MDP with finite state space and finite action space, there is $\lim_{t\to\infty} \frac{1}{t} \cdot \sum_{\tau=0}^{t} \|\mathcal{P}^{(\tau)} - \mathcal{P}\| = 0$ [34], [35]. $\mathcal{P}^{(\tau,\tau+n)}$ denotes a n-step transition matrix, i.e., $\mathcal{P}^{(\tau,\tau+n)} = \mathcal{P}^{(\tau)} \cdot \mathcal{P}^{(\tau+1)} \cdots \mathcal{P}^{(\tau+n)}$. Then, we have the following inequality:

$$\begin{aligned}\|\mathcal{P}^{(\tau,\tau+2)} - \mathcal{P}^2\| &\le \|\mathcal{P}^{(\tau+1)} \cdot \mathcal{P}^{(\tau+2)} - \mathcal{P}^{(\tau+1)} \cdot \mathcal{P}\| \\ &+ \|\mathcal{P}^{(\tau+1)} \cdot \mathcal{P} - \mathcal{P}^2\| \le \|\mathcal{P}^{(\tau+2)} - \mathcal{P}\| \\ &+ \|\mathcal{P}^{(\tau+1)} - \mathcal{P}\|, \end{aligned} \tag{21}$$

which implies that: $\lim_{t\to\infty} \frac{1}{t} \cdot \sum_{\tau=0}^{t} \|\mathcal{P}^{(\tau,\tau+2)} - \mathcal{P}^2\| = 0$.

For any two positive integers k and k', we can obtain that: $\lim_{t\to\infty} \frac{1}{t} \cdot \sum_{\tau=0}^{t} \|\mathcal{P}^{(\tau,\tau+k)} - \mathcal{P}^k\| = 0$ and $\lim_{t\to\infty} \frac{1}{t} \cdot \sum_{\tau=0}^{t} \|\mathcal{P}^{(\tau+k',\tau+k'+k)} - \mathcal{P}^k\| = 0$ by an inductive method, indicating that the MDP model can converge in the Cesàro sense. □

Thus, after a finite number of iterations, the optimal solution can be obtained, i.e., the optimal placements of idle MCSs can be obtained.

Proposition 2: The convergence rate of the MDP model is approximated to a geometric rate.

Proof: Suppose $\mathcal{Q}$ is a constant matrix formed by the rows of left eigenvector of $\mathcal{P}$ (denoted by π). Since the left eigenvector satisfies that $\pi\mathcal{P} = \lambda\mathcal{P}$ and $\sum_i \pi_i = 1$. Then, we can obtain the following inequality similar to [35]:

$$\begin{aligned}\sup_{m\ge 0} \| \frac{1}{t} \sum_{\tau=1}^{t} \mathcal{P}^{(m,m+\tau)} - \mathcal{Q} \| &\le \frac{2(Jd+r)}{t} \\ &+ \sup_{m\ge 0} d \sum_{v=1}^{W+d-1} \frac{1}{t} \sum_{\tau=1}^{t} \| \mathcal{P}_{m+\tau+v} - \mathcal{P} \| \\ &+ \frac{L-J}{t} \| \sum_{\tau=1}^{d} \mathcal{P}^{W+\tau-1} - d\mathcal{Q} \|, \end{aligned} \tag{22}$$

where L, W, and J satisfy that: $t = Ld + r$ $(0 \le r \le d)$ and $W \le Jd \le Ld$.

We have that $\| \sum_{\tau=1}^{d} \mathcal{P}^{W+\tau-1} - d\mathcal{Q} \| \le C\beta^W$ $(C > 0$ and $1 > \beta > 0)$ [34].

Let $W = \frac{-\alpha \ln t + 1}{\ln \beta}$ $(\alpha > 0)$ and $J = W + 1$, there is:

$$\| \sum_{\tau=1}^{d} \mathcal{P}^{W+\tau-1} - d\mathcal{Q} \| \le C\beta^W = Ct^{-\alpha}, \tag{23}$$

which yields that: $\sup_{m\ge 0} \frac{1}{t} \sum_{\tau=1}^{t} \|\mathcal{P}_{m+\tau} - \mathcal{P}\| \le Gt^{-\alpha}$, where G a constant, and then we obtain (24):

$$\begin{aligned}&\sup_{m\ge 0} d \sum_{v=1}^{W+d-1} \frac{1}{t} \sum_{\tau=1}^{t} \| \mathcal{P}_{m+\tau+v} - \mathcal{P} \| \\ &\le d \sum_{v=1}^{W+d-1} Gt^{-\alpha} \le Gd(W+d-1)t^{-\alpha}. \end{aligned} \tag{24}$$

Thus, $\forall \varepsilon > 0$, $\exists D(\varepsilon)$ satisfies (25):

$$\begin{aligned}&\| \frac{1}{t} \sum_{\tau=1}^{t} \mathcal{P}^{(m,m+\tau)} - \mathcal{Q} \| \\ &\le t^{\varepsilon-1} + Ct^{\varepsilon-\alpha} \\ &+ Gd(W+d-1)t^{\varepsilon-\alpha} = \frac{D(\varepsilon)}{t^{\min(\alpha,1)-\varepsilon}}, \end{aligned} \tag{25}$$

which indicates that the convergence rate follows a geometric sequence, and the error between two successive iterations is reduced by a fixed proportion. Hence, the convergence rate is geometric with respect to the number of iterations. □

VII. Performance Evaluations

In this section, the simulation results are provided to evaluate the performance of our proposed PS-IMCS, along with some comparisons with other strategy models (R-COST [6], RLA [22], stationary strategy (SS), and random walk strategy (RWS)).

The simulations are conducted on a real-world taxi dataset originally provided by Didi Corporation [36] which has been modified by us according to the mobile charging scenarios.[2] This dataset contains the GPS trajectories of more than 10,000 taxis during the period from Oct. 1, 2018 to Oct. 31, 2018 in Chengdu city, China. Each GPS trajectory is represented by a sequence of taxi ID, latitudes, longitudes, and timestamps. Note that the passengers of taxis and the drivers of EVs have the similar travel intentions in their daily lives. Thus, this dataset is adopted for our simulations, and we use these taxi trajectories to simulate the movements of EVs.

The initial battery electricity of each EV obeys a normal distribution $N(\mu, \delta^2)$ [37], where the value of μ denotes the average residual battery electricity of EVs, and the value of δ denotes the deviation of residual battery electricity among EVs.

We develop a simulator using Python language, and the simulation results are averaged over 500 runs. The main parameter settings are shown in TABLE II. Note that the parameter values given in TABLE II are taken as the default values, i.e., the default values of parameters are adopted in the following simulations when the parameter values are not explicitly explained.

Firstly, an example is illustrated in Fig. 9 with five MCSs, where the placements of idle MCSs decided by PS-IMCS are marked. Fig. 9 shows that the movements of idle MCSs are guided by the charging demand force, until these MCSs receive and approve the charging requests from EVCs.

A. Proportion of Charged EVCs

The proportion of charged EVCs can reflect the charging experience of EVCs. Fig. 10(a) illustrates the impacts of M and N on the proportion of charged EVCs. The proportion of charged EVCs is decreased with the increase of N, because more EVCs could compete for the charging services of MCSs, and thus more EVCs cannot be charged by MCSs. On the contrary, the proportion of charged EVCs is increased with the increase of M, and the reason is that EVCs are easier to be charged by MCSs when MCSs are deployed more densely.

Furthermore, the proportion of charged EVCs under different μ and δ is observed in Fig. 10(b). μ indicates the

[2]https://github.com/lsspac/manually-synthesizing-trajectories

TABLE II
SIMULATION PARAMETERS

Parameter	Description	Value
N	Number of EVs	600
M	Number of MCSs	40
$\|\boldsymbol{P}\|$	Number of charging parks	50
t_s	Length of each time slot	60 s
R_c	Communication range of each EV and each MCS	1 km
T	Number of time slots in an observation period	60
e_{max}	Maximum battery capacity of each MCS	90 kwh
$\widetilde{D}$	Maximum waiting delay	5 min
χ	Number of virtual layers around an idle MCS	6
ϖ	Charging speed	45 kwh/h
m_s	Travel speed of each EV and each MCS	11.1 m/s
μ	Average residual battery electricity of EVs	15 kwh
μ_{max}	Maximum residual battery electricity of EVs	20 kwh
μ_{min}	Minimum residual battery electricity of EVs	10 kwh
δ	Standard deviation of residual battery electricity	3 kwh
c	Electricity consumption for travelling through a unit distance	0.45 kwh/km
ζ_0	Price of electricity purchased from power grid	1.0/kwh
ζ_c	Price of electricity transferred from an MCS to an EVC	2.4/kwh
γ	Parameter of low battery state	9
κ	Number of input records in Bi-LSTM	10
ς	Discount coefficient	0.8

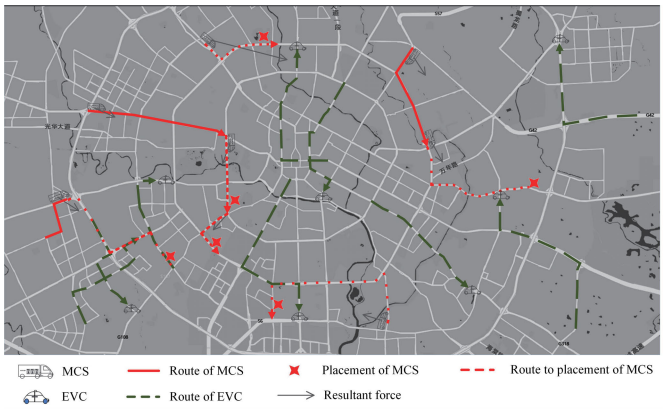

Fig. 9. An example of placements of idle MCSs.

average residual battery electricity of EVs, and the proportion of charged EVCs with a larger μ is larger than that with a smaller μ, due to the fact that a larger μ implies that more EVs have enough battery electricity to complete their travels without charging demand, and thereby EVCs can be charged by MCSs more easily. The proportion of charged EVCs is dropped when δ is increased, and this is because with a larger δ more EVCs have the residual battery electricity which is under the low battery state.

Fig. 10(c) illustrates the impact of $\widetilde{D}$ on the proportion of charged EVCs. $\widetilde{D}$ denotes the maximum time allowing an EVC to be charged by MCSs after it makes a charging request. Thus, the proportion of charged EVCs is gradually increased

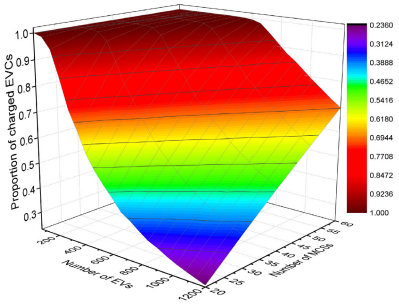

(a) Proportion of charged EVCs vs. M and N

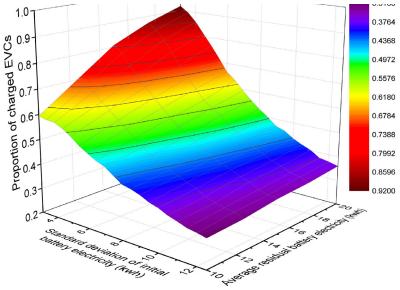

(b) Proportion of charged EVCs vs. μ and δ

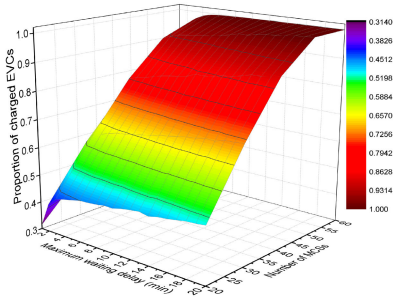

(c) Proportion of charged EVCs vs. M and $\widetilde{D}$

Fig. 10. Proportion of charged EVCs.

with the increase of $\widetilde{D}$, because EVCs are allowed to wait for the arrivals of MCSs during a longer period.

B. Average Charging Delay of EVCs

As shown in Fig. 11(a), the curve with a larger M is much lower than that with a smaller M, which is attributed to the fact that EVCs can be charged more conveniently when more MCSs are deployed, and thus the average charging delay of EVCs is largely shortened. The average charging delay of EVCs is prolonged with the increase of N, and this is because some EVCs could wait longer for the MCSs which should first charge other EVCs.

In Fig. 11(b), the curve with a larger μ is lower than that with a smaller one. The reason is that an EVC with less residual battery electricity typically requires more electricity, thus yielding longer charging time (the third part in (3)). Note that the charging time does not affect the action-decisions of idle MCSs. However, if the charging speed is too slow, the travels of EVCs will be delayed for a longer period due to longer charging time.

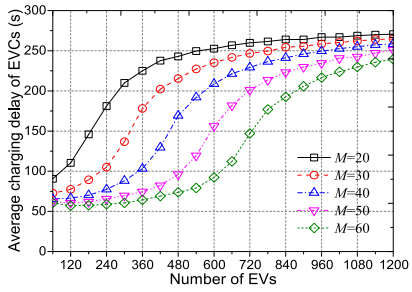

(a) Average charging delay of EVCs vs. M and N

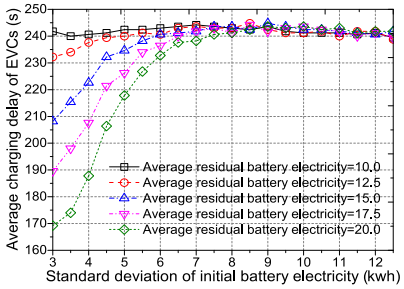

(b) Average charging delay of EVCs vs. μ and δ

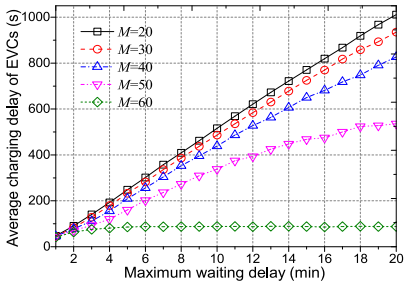

(c) Average charging delay of EVCs vs. M and $\widetilde{D}$

Fig. 11. Average charging delay of EVCs.

Likewise, a smaller δ implies that more EVs have the residual battery electricity exceeding the low battery state, which shortens the average charging delay of EVCs. With a larger $\widetilde{D}$, the average charging delay of EVCs is prolonged (Fig. 11(c)).

C. Impact of Maximum Battery Capacity of Each MCS

The maximum battery capacity of each MCS is set to 90 kwh (TABLE II), i.e., the residual electricity of each MCS is equal to 90 kwh after it is recharged by the power grid. We provide Fig. 12 to observe the impact of the maximum battery capacity of each MCS. In Fig. 12, we find that the proportion of charged EVCs is increased with the increase of e_{max}, because the service time of MCSs is prolonged when each MCS has a larger battery capacity (a larger e_{max}), and thus more EVCs can be charged. When the maximum battery capacity is large enough ($e_{max} > 30$ kwh), the proportion of charged EVCs remains almost unchanged.

Besides, the average charging delay of EVCs is independent of e_{max}, and the reason is that only the charging delay of successfully charged EVCs is counted into the average charging delay of EVCs, and hence the average charging delay of EVCs is mainly related to the deployment density of MCSs (i.e. the number of MCSs) rather than the maximum battery capacity.

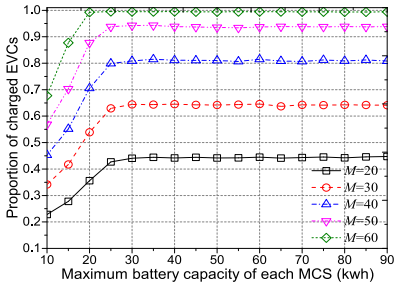

(a) Proportion of charged EVCs vs. e_{max}

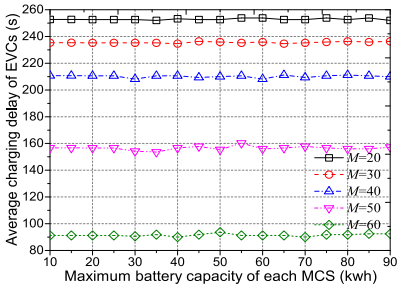

(b) Average charging delay of EVCs vs. e_{max}

Fig. 12. Impact of maximum battery capacity of each MCS.

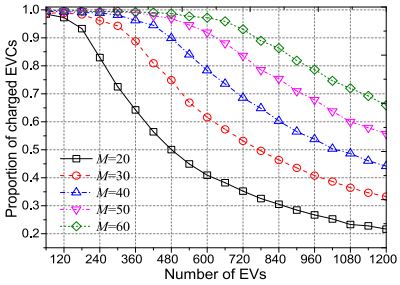

(a) Proportion of charged EVCs vs. M and N

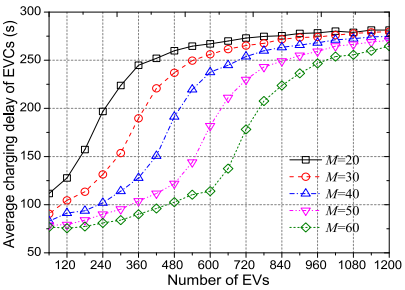

(b) Average charging delay of EVCs vs. M and N

Fig. 13. Simulation results on a synthetic dataset.

D. Proportion of Charged EVCs and Average Charging Delay of EVCs on a Synthetic Dataset

We manually synthesize a small dataset which consists of 20,000 trajectories, and each trajectory is composed of a series of longitudes, latitudes, and timestamps. The initial positions of the trajectories are uniformly distributed in the longitude interval [104.031,104.129] and the latitude interval [30.631,30.729]. The location of each EV is sampled every minute to form these trajectories. The simulation results in terms of proportion of charged EVCs and average charging delay of EVCs conducted on this dataset are given in Fig. 13. Similar to the results in Fig. 10(a) and Fig. 11(a), the proportion of charged EVCs is decreased with the increase of N and

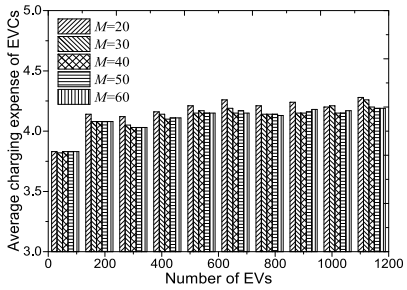

(a) Average charging expense of EVCs vs. M and N

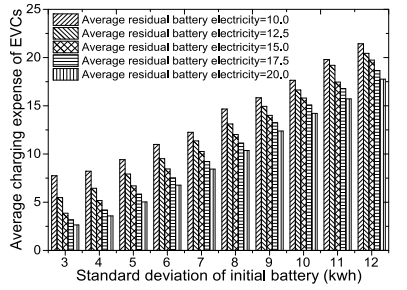

(b) Average charging expense of EVCs vs. μ and δ

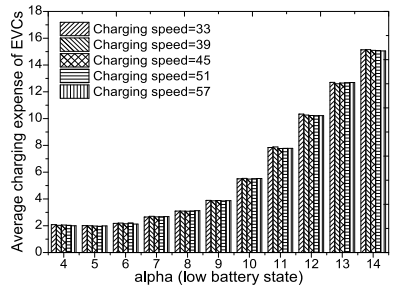

(c) Average charging expense of EVCs vs. ϖ and γ

Fig. 14. Average charging expense of EVCs.

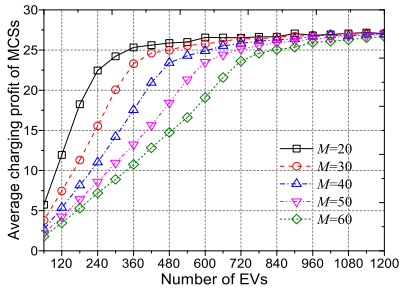

(a) Average charging profit of MCSs vs. M and N

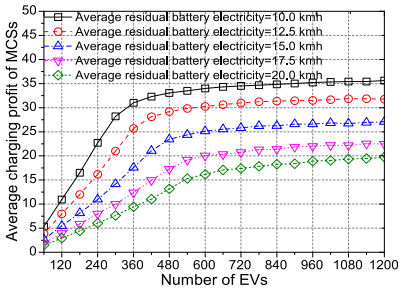

(b) Average charging profit of MCSs vs. μ and N

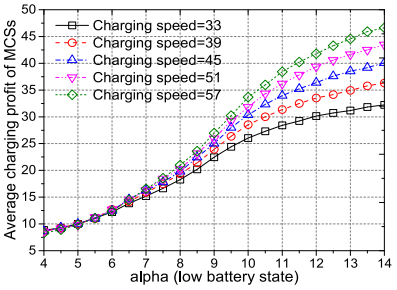

(c) Average charging profit of MCSs vs. ϖ and γ

Fig. 15. Average charging profit of MCSs.

increased with the increase of M. The average charging delay of EVCs is increased with the increase of N and decreased with the increase of M.

E. Average Charging Expense of EVCs

The charging expense of an EVC is calculated as [21]. Fig. 14 illustrates the impacts of M, N, μ, δ, ϖ, and γ on the average charging expense of EVCs. Two observations are obtained: (i) The number of MCSs does not have an obvious impact on the average charging expense of EVCs, because the average charging expense of EVCs is calculated as the average of the charging expenses of EVCs which have been charged by MCSs, rather than those EVCs which cannot be charged during the maximum waiting delay $\widetilde{D}$; (ii) The average charging expense of EVCs is slowly increased with the increase of N, due to the intensified competitions among EVCs for MCSs.

In Fig. 14(b), the average charging expense of EVCs is reduced with the increase of μ or the decrease of δ, which is attributed to the fact that a larger μ or a smaller δ indicates that less electricity is required by EVCs.

When γ is set smaller, EVCs make charging requests earlier, and they could be charged by MCSs with shorter extra travels (Fig. 14(c)), thus reducing their charging expenses. Fig. 14(c) also indicates that the average charging expense of EVCs is almost independent of ϖ, i.e., the charging speed does not affect the charging expenses of EVCs.

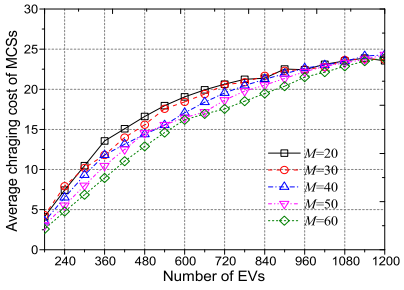

Fig. 16. Average charging cost of MCSs.

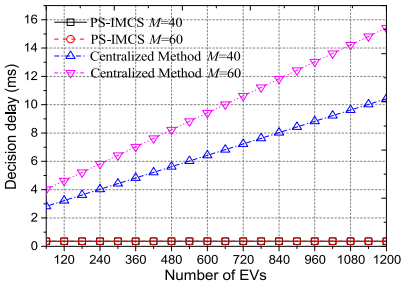

Fig. 17. Decision delay.

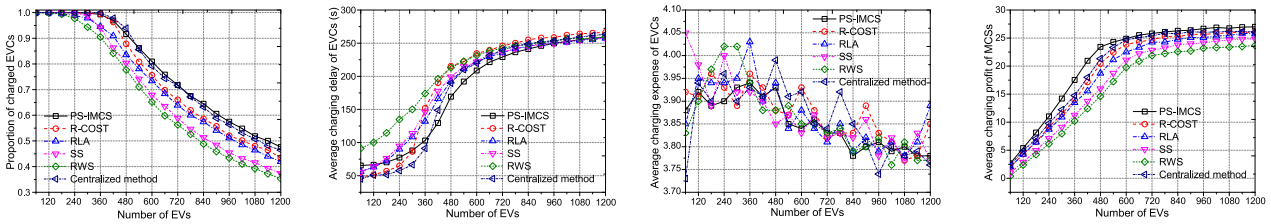

(a) Proportion of charged EVCs (b) Average charging delay of EVCs (c) Average charging expense of EVCs (d) Average charging profit of MCSs

Fig. 18. Comparisons among different strategy models.

F. Average Charging Profit of MCSs and Average Charging Cost of MCSs

The average charging profit of MCSs [38] reflects the charging efficiency of MCSs. Essentially, the charging profit of an MCS can be raised by prolonging the charging duration, i.e., an MCS earns a larger profit by spending more time on charging EVCs rather than travelling on the roads.

In Fig. 15(a), we observe that the curves of average charging profit of MCSs first ascend rapidly with the increase of N, and then these curves grow slowly when N is large enough ($N \geq 720$), due to the fact that the number of EVCs which can be served by MCSs remains constant when there are a large number of EVCs (the charging capacity of MCSs is related to the number of MCSs), although MCSs can earn more charging profits by charging more EVCs. The average charging profit of MCSs is larger with a smaller M (when N is small), and the reason is that the average charging profit of MCSs can be increased by making each MCS undertake the charging tasks as more as possible. The above phenomena indicate that the number of MCSs should be carefully arranged according to the number of EVs, and thus a proper tradeoff between the charging profits of MCSs and the deployment cost of MCSs can be achieved.

Likewise, the decrease of μ (EVCs require more electricity) leads to the increase of the average charging profit of MCSs, as shown in Fig. 15(b).

In Fig. 15(c), if MCSs can charge EVCs more quickly (a larger ϖ), and then MCSs can charge more EVCs and earn more charging profits. A larger γ implies that EVCs make the charging requests when they have less residual electricity, and MCSs should transfer more electricity to EVCs.

The average charging cost of MCSs is calculated as the average of the cost for travelling on roads of all MCSs. As shown in Fig. 16, the average charging cost of MCSs is increased with the increase of N, the reason is that when M is fixed (the number of MCSs is fixed) there are more EVCs when there are more EVs distributed in the road network, and idle MCSs could charge more EVCs (the average charging profit of MCSs is increased) with larger cost, although idle MCSs could be closer to EVCs when there are more EVs distributed in the road network.

G. Comparisons Among Different Strategy Models

Firstly, we compare PS-IMCS with the centralized method (a centralized version of PS-IMCS) in terms of the decision delay. In the centralized method, the cloud server obtains the information of all EVCs and MCSs (the current positions and required electricity of all EVCs, the current positions and residual electricity of all idle MCSs), and makes the placement decisions for idle MCSs. The decision delay is comprised of three parts: the delay for predicting the amount of required electricity of EVCs on road segments, the communication delay, and the delay for carrying out the MDP model.

The simulation results of the decision delay are provided in Fig. 17, which indicates that the decision delay of PS-IMCS is significantly shorter than that of the centralized method, and the decision delay of PS-IMCS is prolonged very slightly with the increase of the number of EVs.

To further analyze the merits of PS-IMCS, we compare PS-IMCS with R-COST, RLA, SS, RWS, and centralized method. These strategy models are compared in terms of the proportion of charged EVCs, average charging delay of EVCs, average charging expense of EVCs, and average charging profit of MCSs. The simulation results are given in Fig. 18, which suggests that PS-IMCS can achieve superior results and outperform other strategy models.

The reason for these phenomena is that PS-IMCS can make appropriate placement decisions for idle MCSs by the adopted attraction-repulsion model which depicts the interaction between charging demand and charging supply over time, and idle MCSs can track the EVCs with large charging demand and move into the areas with few idle MCSs. Thus, idle MCSs can charge EVCs more agilely once EVCs make charging requests.

Specially, RWS yields the smallest proportion of charged EVCs, the longest average charging delay of EVCs, and the smallest average charging profit of MCSs, which suggests that the random walks of idle MCSs worsen the charging efficiency of MCSs significantly. In Fig. 18(a), the curves of different strategy models are close to each other and have some fluctuations with the increase of N.

The average charging delay of EVCs obtained by R-COST is shorter than that of PS-IMCS when $N \leq 300$, because R-COST adopts a centralized method to obtain better placements for idle MCSs. However, with the further increase of N, the potential charging demand and charging supply are much difficult to be predicted, and accordingly the placements of idle MCSs are difficult to be properly decided, although a centralized method is adopted. Moreover, a centralized method is not available in real charging scenarios due to the extremely high communication complexity and computational complexity.

Note that the performance of PS-IMCS is better than that of the centralized method. This is because the placement decisions of idle MCSs are decided based on the charging demand force, and in the centralized method the charging demand force around each idle MCS is affected by all EVCs and other idle MCSs. Actually, the idle MCSs far away from EVCs cannot provide the charging services, and the calculation of charging demand force in the centralized method cannot reflect the charging demand and charging supply around each idle MCS properly.

VIII. Conclusion

We have studied the problem of placements of idle MCSs, and the Placement Strategy for Idle Mobile Charging Stations (PS-IMCS) has been introduced. In PS-IMCS, each idle MCS can measure the potential charging demand in the neighboring area through obtaining the resultant force (charging demand force) composed of attraction force (neighboring EVCs) and repulsion force (neighboring idle MCSs). Moreover, an MDP model is designed to make placement decisions for each idle MCS, and the MDP model can converge to an equilibrium quickly. Therefore, PS-IMCS reduces the charging delay of EVCs and enhances the proportion of charged EVCs effectively.

The length of each time slot should be properly set. If the length of each time slot is too long, the potential charging demand of EVCs cannot be timely measured, and the placements of idle MCSs will be less efficient; If the length of each time slot is too short, both the communication complexity and computational complexity of PS-IMCS will be increased due to more frequent communications and computations, and the action decision of each idle MCS could not be completed during a time slot. In PS-IMCS the charging services of MCSs are provided based on the FCFS principle (First Come First Service). However, the performance of PS-IMCS can be further improved, if some EVCs making charging requests later are allowed to be charged earlier (e.g., these EVCs are nearer to idle MCSs, or the maximum waiting delay of these EVCs is about to expire). This work mainly focuses on the placements of idle MCSs, and FCSs are not considered in the model and the proposed strategy. FCSs can be considered as special MCSs which are stationary, i.e., the moving speed of FCSs is equal to zero. Thereby, PS-IMCS can be evolved into a strategy suitable for the IoEV with both FCSs and MCSs.

References

[1] H. S. Das et al., "Electric vehicles standards, charging infrastructure, and impact on grid integration: A technological review," *Renew. Sustain. Energy Rev.*, vol. 120, Mar. 2020, Art. no. 109618.

[2] M. Ehsani, K. V. Singh, H. O. Bansal, and R. T. Mehrjardi, "State of the art and trends in electric and hybrid electric vehicles," *Proc. IEEE*, vol. 109, no. 6, pp. 967–984, Jun. 2021.

[3] L. Park, S. Jeong, D. S. Lakew, J. Kim, and S. Cho, "New challenges of wireless power transfer and secured billing for Internet of Electric Vehicles," *IEEE Commun. Mag.*, vol. 57, no. 3, pp. 118–124, Mar. 2019.

[4] H. Zhang et al., "Optimized scheduling for urban-scale mobile charging vehicle," in *Proc. 2nd World Symp. Commun. Eng. (WSCE)*, Nagoya, Japan, Dec. 2019, pp. 164–172.

[5] S. Afshar et al., "Mobile charging stations for electric vehicles—A review," *Renew. Sustain. Energy Rev.*, vol. 152, Dec. 2021, Art. no. 111654.

[6] X. Zhang, Y. Cao, L. Peng, J. Li, N. Ahmad, and S. Yu, "Mobile charging as a service: A reservation-based approach," *IEEE Trans. Autom. Sci. Eng.*, vol. 17, no. 4, pp. 1976–1988, Oct. 2020.

[7] M. S. H. Lipu, M. A. Hannan, A. Hussain, M. H. Saad, A. Ayob, and M. N. Uddin, "Extreme learning machine model for state-of-charge estimation of lithium-ion battery using gravitational search algorithm," *IEEE Trans. Ind. Appl.*, vol. 55, no. 4, pp. 4225–4234, Jul. 2019.

[8] G. Gruosso, A. Mion, and G. S. Gajani, "Forecasting of electrical vehicle impact on infrastructure: Markov chains model of charging stations occupation," *eTransportation*, vol. 6, Nov. 2020, Art. no. 100083.

[9] G. Ferro, R. Minciardi, L. Parodi, and M. Robba, "Optimal planning of charging stations in coupled transportation and power networks based on user equilibrium conditions," *IEEE Trans. Autom. Sci. Eng.*, vol. 19, no. 1, pp. 48–59, Jan. 2022.

[10] L. V. Wahl, N. Tempelmeier, A. Sao, and E. Demidova, "Reinforcement learning-based placement of charging stations in urban road networks," in *Proc. 28th ACM SIGKDD Conf. Knowl. Discovery Data Mining (KDD)*, 2022, pp. 3992–4000.

[11] Q. Chen et al., "Dynamic price vector formation model-based automatic demand response strategy for PV-assisted EV charging stations," *IEEE Trans. Smart Grid*, vol. 8, no. 6, pp. 2903–2915, Nov. 2017.

[12] J. Antoun, M. E. Kabir, R. F. Atallah, and C. Assi, "A data driven performance analysis approach for enhancing the QoS of public charging stations," *IEEE Trans. Intell. Transp. Syst.*, vol. 23, no. 8, pp. 11116–11125, Aug. 2022.

[13] R. Xie, W. Wei, Q. Wu, T. Ding, and S. Mei, "Optimal service pricing and charging scheduling of an electric vehicle sharing system," *IEEE Trans. Veh. Technol.*, vol. 69, no. 1, pp. 78–89, Jan. 2020.

[14] W. Zhang et al., "Multi-agent graph convolutional reinforcement learning for dynamic electric vehicle charging pricing," in *Proc. 28th ACM SIGKDD Conf. Knowl. Discovery Data Mining (KDD)*, 2022, pp. 2471–2481.

[15] C. Wang, X. Lin, F. He, M. Z.-J. Shen, and M. Li, "Hybrid of fixed and mobile charging systems for electric vehicles: System design and analysis," *Transp. Res. C, Emerg. Technol.*, vol. 126, May 2021, Art. no. 103068.

[16] S. Jeon and D. H. Choi, "Optimal energy management framework for truck-mounted mobile charging stations considering power distribution system operating conditions," *Sensors*, vol. 21, no. 8, p. 2798, 2021.

[17] N. Chen, M. Li, M. Wang, J. Ma, and X. Shen, "Compensation of charging station overload via on-road mobile energy storage scheduling," in *Proc. IEEE Global Commun. Conf. (GLOBECOM)*, Waikoloa, HI, USA, Dec. 2019, pp. 1–6.

[18] S. Cui, X. Ma, M. Zhang, B. Yu, and B. Yao, "The parallel mobile charging service for free-floating shared electric vehicle clusters," *Transp. Res. E, Logistics Transp. Rev.*, vol. 160, Apr. 2022, Art. no. 102652.

[19] M. S. Răboacă, I. Băncescu, V. Preda, and N. Bizon, "An optimization model for the temporary locations of mobile charging stations," *Mathematics*, vol. 8, no. 3, p. 453, 2020.

[20] P. Zhong, A. Xu, J. Gao, Y. Zhang, and Y. Chen, "An efficient on-demand charging scheduling scheme for mobile charging vehicle," *Int. J. Commun. Syst.*, vol. 34, no. 13, 2021, Art. no. e4919.

[21] L. Liu, X. Qi, Z. Xi, J. Wu, and J. Xu, "Charging-expense minimization through assignment rescheduling of movable charging stations in electric vehicle networks," *IEEE Trans. Intell. Transp. Syst.*, vol. 23, no. 10, pp. 17212–17223, Oct. 2022.

[22] J. Ni, R. Liang, and H. Wu, "Collaborative mobile charging vehicles placement: A reinforcement learning approach," in *Proc. IEEE 23rd Int Conf High Perform. Comput. Commun.*, Haikou, China, Dec. 2021, pp. 920–926.

[23] J. Qiu and L. Du, "Optimal dispatching of electric vehicles for providing charging on-demand service leveraging charging-on-the-move technology," *Transp. Res. C, Emerg. Technol.*, vol. 146, Jan. 2023, Art. no. 103968.

[24] H. R. Sayarshad and J. Y. Chow, "Non-myopic relocation of idle mobility-on-demand vehicles as a dynamic location-allocation-queueing problem," *Transp. Res. E, Logistics Transp. Rev.*, vol. 106, pp. 60–77, Oct. 2017.

[25] X. Liu, J. Y. J. Chow, and S. Li, "Online monitoring of local taxi travel momentum and congestion effects using projections of taxi GPS-based vector fields," *J. Geograph. Syst.*, vol. 20, pp. 253–274, Jul. 2018.

[26] T. P. Pantelidis, L. Li, T.-Y. Ma, J. Y. J. Chow, and S. E. G. Jabari, "A node-charge graph-based online carshare rebalancing policy with capacitated electric charging," *Transp. Sci.*, vol. 56, no. 3, pp. 654–676, 2022.

[27] K. Kang, D. Kim, and S.-O. Yang, "Existence of generalized solutions to an attraction-repulsion Keller–Segel system with degradation," *J. Math. Anal. Appl.*, vol. 511, no. 1, 2022, Art. no. 126069.
[28] A. Baykasoğlu and C. Baykasoğlu, "Weighted superposition attraction-repulsion (WSAR) algorithm for truss optimization with multiple frequency constraints," *Structures*, vol. 30, pp. 253–264, Apr. 2021.
[29] L. A. Márquez-Vega, M. Aguilera-Ruiz, and L. M. Torres-Treviño, "Multi-objective optimization of a quadrotor flock performing target zone search," *Swarm Evol. Comput.*, vol. 60, Feb. 2021, Art. no. 100733.
[30] M. Wu, S. Pan, and X. Zhu, "Attraction and repulsion: Unsupervised domain adaptive graph contrastive learning network," *IEEE Trans. Emerg. Topics Comput. Intell.*, vol. 6, no. 5, pp. 1079–1091, Oct. 2022, doi: 10.1109/TETCI.2022.3156044.
[31] V. Kumar, "Mathematical analysis of reinforcement learning—Bellman optimality equation," *Towards Data Sci.*, pp. 1–13, Feb. 2020.
[32] H. Xue, D. Q. Huynh, and M. Reynolds, "PoPPL: Pedestrian trajectory prediction by LSTM with automatic route class clustering," *IEEE Trans. Neural Netw. Learn. Syst.*, vol. 32, no. 1, pp. 77–90, Jan. 2021.
[33] P. J. Freire et al., "Performance versus complexity study of neural network equalizers in coherent optical systems," *J. Lightw. Technol.*, vol. 39, no. 19, pp. 77–90, Oct. 2021.
[34] B. Bowerman, H. T. David, and D. Isaacson, "The convergence of Cesaro averages for certain nonstationary Markov chains," *Stochastic Processes Appl.*, vol. 5, no. 3, pp. 221–230, 1977.
[35] W. Yang, "Convergence in the Cesàro sense and strong law of large numbers for nonhomogeneous Markov chains," *Linear Algebra Appl.*, vol. 354, nos. 1–3, pp. 275–288, Oct. 2002.
[36] Didi Corporation. (2020). *GAIA Open Dataset*. [Online]. Available: https://outreach.didichuxing.com/app-vue/dataList
[37] R. R. Richardson, M. A. Osborne, and D. A. Howey, "Gaussian process regression for forecasting battery state of health," *J. Power Sources*, vol. 357, pp. 209–219, Jul. 2017.
[38] L. Liu, H. Zhang, J. Xu, and P. Wang, "Providing active charging services: An assignment strategy with profit-maximizing heat maps for idle mobile charging stations," *IEEE Trans. Mobile Comput.*, early access, Feb. 22, 2023, doi: 10.1109/TMC.2023.3247441.

Linfeng Liu (Member, IEEE) received the B.S. and Ph.D. degrees in computer science from Southeast University, Nanjing, China, in 2003 and 2008, respectively. He is currently a Professor with the School of Computer Science and Technology, Nanjing University of Posts and Telecommunications, China. He has published more than 120 peer-reviewed papers in some technical journals or conference proceedings, such as IEEE TRANSACTIONS ON MOBILE COMPUTING, IEEE TRANSACTIONS ON PARALLEL AND DISTRIBUTED SYSTEMS, IEEE TRANSACTIONS ON INFORMATION FORENSICS AND SECURITY, IEEE TRANSACTIONS ON INTELLIGENT TRANSPORTATION SYSTEMS, IEEE TRANSACTIONS ON VEHICULAR TECHNOLOGY, IEEE TRANSACTIONS ON SERVICES COMPUTING, *ACM TAAS*, *ACM TOIT*, *Computer Networks*, and *JPDC* (Elsevier). His main research interests include vehicular ad hoc networks, wireless sensor networks, and multi-hop mobile wireless networks. He has served as a TPC Member for GLOBECOM, ICONIP, VTC, and WCSP.

Su Liu received the B.S. degree in applied physics from the Nanjing University of Information Science and Technology in 2021. He is currently pursuing the master's degree with the Nanjing University of Posts and Telecommunications. His current research interests include the Internet of Electric Vehicles and vehicular ad hoc networks.

Jiagao Wu (Member, IEEE) received the Ph.D. degree in computer science from Southeast University, Nanjing, China, in 2006. He is currently an Associate Professor with the School of Computer Science and Technology, Nanjing University of Posts and Telecommunications. His current research interests include mobile social networks and opportunistic networks.

Jia Xu (Senior Member, IEEE) received the Ph.D. degree from the School of Computer Science and Engineering, Nanjing University of Science and Technology, Jiangsu, China, in 2010. He is currently a Professor with the Jiangsu Key Laboratory of Big Data Security and Intelligent Processing, Nanjing University of Posts and Telecommunications. His main research interests include crowdsourcing, edge computing, and wireless sensor networks. He has served as a TPC Member for GLOBECOM, ICC, MASS, ICNC, and EDGE. He has served as the PC Co-Chair for SciSec 2019, an Organizing Chair for ISKE 2017, and the Publicity Co-Chair for SciSec 2021.